Crystal and Electronic Structure of the Novel Layered Rare Earth Metal Boride Carbide $Gd_2B_3C_2$

Fabrice Wiitkar,[†] Jean-François Halet,*[,†] Jean-Yves Saillard,*[,†] Peter Rogl,*[,‡] and Josef Bauer*[,§]

Laboratoire de Chimie du Solide et Inorganique Moléculaire, URA CNRS 1495, Université de Rennes I, 35042 Rennes Cedex, France, Institut für Physikalische Chemie, Universität Wien, Währingerstrasse 42, A-1090 Wien, Austria, and Laboratoire de Chimie du Solide et Inorganique Moléculaire, URA CNRS 1495, Institut National des Sciences Appliquées, 35043 Rennes Cedex, France

Received July 23, 1993[⊗]

The crystal structure of $Gd_2B_3C_2$ has been determined from single-crystal X-ray counter data. $Gd_2B_3C_2$ crystallizes in a unique structure type with the orthorhombic space group $Cmmm$-D_{2h}^{19}, No. 65, $Z = 2$. The lattice parameters are $a = 0.3445(1)$, $b = 1.3733(3)$, and $c = 0.37107(7)$ nm. The structure was solved by combined Patterson–difference Fourier methods and refined by full-matrix least-squares calculation. $R_F = \sum|\Delta F|/\sum|F_o| = 0.053$ for an asymmetric set of 246 independent reflections ($|F_o| > 3\sigma(|F_o|)$). Boron atoms in triangular metal coordination form infinite zigzag chains branched with carbon atoms. Boron atoms are at a distance of d(B1–B1) = 0.1920 nm with a bond angle of $\varphi_{B1-B1-B1} = 127.6°$. Branched carbon atoms in 4-fold rectangular metal coordination are at a distance d(B1–C) = 0.1597 nm from the B–B chain under bond angles $\varphi_{C-B1-B1} = 116.2°$. The boron chains are linked to a planar two-dimensional boron–carbon network by additional boron atoms forming rather tight bonds with the branched carbon atoms at distances of d(B2–C) = 0.1413 nm under bond angles $\varphi_{C-B2-C} = 180°$. With respect to the structural chemical building blocks and near neighbors, the crystal structure of $Gd_2B_2^{[6Gd+C,2]}B^{[2C,-]}C_2^{[4Gd+2B,-]}$ is related to the structure type of $YB^{[6Y+C,2]}C^{[4Y+B,-]}$, which lacks the nonmetal atom linking the carbon-branched boron zigzag chains. The electronic structure and bonding properties of $Gd_2B_3C_2$ are analyzed by means of extended Hückel tight-binding calculations. The results show that an ionic picture between the metallic and the boron–carbon sublattices is a good starting point to explain the arrangement observed in the nonmetal framework. Thus, a formal charge of 5- per B_3C_2 unit accounts for the boron–carbon structural arrangement of the B–C net in $Gd_2B_3C_2$. The electronic structure of the anionic two-dimensional boron–carbon layers is found to be strongly related to that of the boron–carbon layers encountered in ThB_2C and α-UB_2C structures. The possibility of B–B bond alternation is discussed. In the three-dimensional material, the metal–nonmetal bonding occurs primarily through electron donation from the anionic sublattice toward the metallic elements, leading to a metallic behavior.

Introduction

The formation of ternary and higher order transition metal boride carbides is directly linked with the electron donor capacity of the transition metal to stabilize the naturally electron-deficient boron-carbon aggregation[1] resulting in a structural chemistry particularly rich in differentiated structure types for the rare earth (RE) metals,[2] the actinoid metals[3] and for the alkaline earth metals. Information on the phase relations in ternary rare earth–boron–carbon systems still is scarce and polythermal projections of the phase relations as obtained from arc melted samples are only available for Y–B–C,[4] La–B–C,[5] Ce–B–C,[6,7] Eu–B–C,[8] Gd–B–C,[9] Ho–B–C,[10] and Er–B–C.[11]

With respect to our interest in boron–carbon network formation, this paper is particularly devoted to the crystal and electronic structure of the compound first discovered and labeled "$Gd_{30}B_{40}C_{30}$" by Smith and Gilles[9] and later described as "GdBC" with the YBC-type by Bauer and Debuigne.[12]

Experimental Section

(a) Preparation. Alloys with a nominal composition GdBC, GdB_2C, $Gd_2B_3C_2$, and $Gd_2B_2C_3$, each weighting ca. 1 g, were prepared by argon arc melting ingots of elemental Gd (purity 99.9 mass% Gd, Cerac, USA) and compacted blends of boron (99.8%, H. C. Starck) and carbon powders (reactor grade, impurities <1.5 ppm, Carbone Lorraine). To ensure homogeneity, the alloy buttons were turned over and remelted several times; weight losses were checked to be within 1% of the original mass. For subsequent annealing at 1000 °C, the alloys contained in cylindrical Knudsen-type carbon crucibles were heated for 48 h in a tungsten sheet metal high-vacuum furnace at 10^{-4} Pa.

For metallographic inspection some of the alloy buttons were mounted in epoxy resin, ground on silicon carbide paper and diamond wheels and subsequently polished on a nylon cloth using diamond paste of consecutively finer grain size (down to 1/4 μm) and finally examined on a Reichert optical microscope under reflected and polarized light. Due to the sensitivity to moisture, all metallographic preparations were performed under water-free protective oil.

Precise lattice parameters and standard deviations were obtained by a least squares refinement of room-temperature Guinier-Huber and 114.59 nm Debye-Scherrer X-ray powder data, using monochromatized Cu $K\alpha_1$ radiation with an internal standard of 99.9999% pure Ge ($a_{Ge} = 0.5657906$ nm).

A small crystal fragment in the form of a trapezoid platelet bound by the crystal faces (100) (260 μm), ($\bar{1}$10) (228 μm), (110) (115 μm) and

† Université de Rennes I.
‡ Universität Wien.
§ Institut National des Sciences Appliquées.
⊗ Abstract published in *Advance ACS Abstracts,* February 15, 1994.

(1) Wiitkar, F.; Halet, J.-F.; Saillard, J.-Y.; Bauer, J.; Rogl, P. *J. Am. Chem. Soc.* **1994**, *116*, 251.
(2) Bauer, J. New Rare Earth Borocarbides. In *Boron-rich Solids, AIP Conference Proceedings 231, Albuquerque, New Mexico, USA* **1990**; Emin, D., *et al.*, Eds.; AIP: New York, 1991; p 216.
(3) Rogl, P. Actinoid Metal Boron Carbides. In *The Physics and Chemistry of Carbides, Nitrides and Borides*; Freer, R., Ed.; Kluwer Acad. Publ.: Dordrecht, Boston, MA, London, 1992; pp 269–277.
(4) Bauer, J.; Nowotny, H. *Monatsh. Chem.* **1971**, *102*, 1129.
(5) Larech, M. Crystal Chemical Investigation of the Ternary System: La–B–C. Thesis, INSA-Rennes, France, 1990.
(6) Brewer, L.; Haraldsen, H. *J. Electrochem. Soc.* **1955**, *102*, 399.
(7) (a) Bonhomme, F.; Gosselin, P. Crystal Chemical Investigation of the Ternary System: Ce-B-C. Thesis, INSA-Rennes, France, 1988. (b) Bauer, J.; Ansel, D.; Bonhomme, F.; Gosselin, P. *J. Less-Common Met.* **1990**, *157*, 109.
(8) Schwetz, K. A.; Hoerle, M.; Bauer, J. *Ceramurgia Int.* **1979**, *5* (3), 105.
(9) Smith, P. K.; Gilles, P. W. *J. Inorg. Nucl. Chem.* **1967**, *29*, 375.
(10) Bauer, J.; Vennegues, P.; Vergneau, J.-L. *J. Less-Common Met.* **1985**, *110*, 295.
(11) Bauer, J. *Proceedings of the 8th International Conference on Solid Compounds of Transition Elements, April 1985*; Wien, Austria, 1985.
(12) Bauer, J.; Debuigne, J. *C. R. Acad. Sci. (Paris) Ser. C* **1972**, *274*, 1271.

0020-1669/94/1333-1297$04.50/0 © 1994 American Chemical Society

Table 1. Crystallographic Data for $Gd_2B_3C_2$ ($Gd_2B_3C_2$-Type)

space group: Cmmm-D_{2h}^{19}, No. 65, origin at $\bar{1}$	
a = 0.3445(1) nm	λ = 0.0710 73 nm
b = 1.3733(3) nm	T = 21 °C
c = 0.37107(7) nm	ρ_{calc} = 7.02 g.cm^{-3}
V = 0.1755 nm^3	μ = 356 cm^{-1}
Z = 2	R^a = 0.053
fw = 370.955	R_w^b = 0.051

^{a} $R = \sum[|F_o| - |F_o|]$. ^{b} $R_w = [\sum w[|F_o| - |F_o|]^2/\sum_w|F_o|^2]^{1/2}$; $w = \sigma F^{-2}$.

Table 2. Atomic Parameters for $Gd_2B_3C_2$

atom	site	occ	x	y	z	U_{eq},[a] Å^0
Gd	**4i**	1.00	0	0.1343(1)	0	0.70(4)
B1	**4j**	1.00	0	0.7191(15)	0.5	1.55(4)
B2	**2c**	1.00	0	0.5	0.5	1.66(6)
C	**4j**	1.00	0	0.6029(15)	0.5	0.78(3)

[a] Equivalent isotropic U defined as $^1/_3(U_{11} + U_{22} + U_{33})$.

Table 3. Interatomic Distances (nm) and Bond Angles (deg) in $Gd_2B_3C_2$

Interatomic Distances

Gd–2Gd	0.3711(0)	B1–4Gd	0.279(1)	C–4Gd	0.257(1)
Gd	0.3690(3)	2Gd	0.274(3)	1B1	0.159(5)
2Gd	0.3613(3)	2B1	0.192(3)	1B2	0.141(3)
2Gd	0.3445(0)	1C	0.159 (5)		
4B1	0.279(1)				
2B1	0.274(3)	B2–2C	0.141(3)		
4C	0.257(1)				

Bond Angles

B1–B1–B1 = 127.6(9) C–B1–B1 = 116.2(8)
C–B2–C = 180.0

($\bar{1}\bar{1}0$) (160 μm) with a thickness of 55 μm (001, 00$\bar{1}$) was broken from a well-crystallized specimen inside a small cavity of the arc melted and annealed button. X-ray intensity data were collected at room temperature on an automatic STOE four-circle diffractometer for one hemisphere of the reciprocal space out to a limit of $(\sin\theta)/\lambda$ = 8.1 nm^{-1} using monochromatized Mo Kα_1 radiation. A set of 253 symmetry independent reflections was obtained by averaging symmetry equivalent reflections out of a total number of 1300 recorded intensities; all observed intensities (246 for $|F_o| > 3\sigma(|F_o|)$) were used in the structure refinement. A geometrical absorption correction has been applied on the crystal fragment described by the six crystal faces mentioned above. The crystallographic data are gathered in Table 1.

(b) Structure Determination. Laue and Weissenberg photographs taken along [101] and [001] revealed orthorhombic lattice geometry without any detectable superstructure reflections. The only observed systematic extinctions were those of a *C*-centered Bravais lattice compatible with one of the following space groups: *Cmmm*, *Cmm2* or *C*222. As statistical tests for the existence of a center of symmetry were not conclusive, solutions were first attempted in the highest symmetry space group *Cmmm*. The interpretation of the Patterson map $P(u,v,w)$ was found to be consistent with Gd atoms in **4i** (0,0.135,0), B1 atoms in **4j** (0,0.719,0.5) and carbon atoms in **4j** (0,0.600,0.5). This structural model, so far identical with the YBC-type,[4] was refined satisfactorily by employing the STRUCSY full-matrix least-squares program system (STOE&CIE, Darmstadt, FRG). A difference map, calculated at this stage $F_o - F_{Gd,B1,C}$ immediately revealed additional maxima corresponding to one additional nonmetal atom in the **2c** sites at (0,0.5,0.5). The weights used for further refinement were based upon counting statistics $w_i = 1/(\sigma(F_i))^2$, and structure factors were furthermore corrected for isotropic secondary extinction. Different weighting schemes had no significant influence on the R values obtained. The refinement of the atom occupancies did not reveal any significant deviation from full occupation and B and C site distribution was suggested from interatomic B–C distances and with respect to reasonable temperature factors. The final R values calculated with anisotropic thermal parameters for Gd but isotropic thermal parameters for B and C were R = 0.053, R_w = 0.051. At this stage a final electron density difference map was featureless, thereby confirming the composition $Gd_2B_3C_2$. Positional and thermal parameters are listed in Table 2. Interatomic distances up to 0.4 nm are given in Table 3. A listing of F_o and F_c data is available upon request. Attempts to refine the crystal structure in lower symmetry in order to release the constraint of equal B1–B1 distances in a similar way as recently discovered for $UB_{0.78}C_{1.22}$ from neutron diffraction[13] were unsuccessful in as far as no further improvement of the residual values could be achieved.

(c) Electronic Band Structure Calculations. All the molecular and tight-binding[14] calculations were carried out within the extended Hückel formalism[15] using standard atomic parameters for B and C. The exponent (ζ) and the valence shell ionization potential (H_{ii} in eV) were, respectively, as follows: 1.3, –15.2 for B 2s; 1.3, –8.5 for B 2p; 1.625, –21.4 for C 2s; 1.625, –11.4 for C 2p; 2.14, –7.42 for Gd 6s; 2.08, –4.65 for Gd 6p. The H_{ii} for Gd 5d was set equal to –8.08 eV. A linear combination of two Slater-type orbitals of exponents ζ_1 = 3.78 and ζ_2 = 1.381 with weighting coefficients c_1 = 0.7765 and c_2 = 0.4586 was used to represent the 5d atomic orbitals of Gd. The 4f orbitals of the lanthanide elements are contracted and low in energy, and it is generally believed that they play a minor role in the chemical bonding. Therefore, they have not been introduced in the calculations. Unless specified in the text, all the considered interatomic distances are the experimental ones. The B–H bond distances used in the molecular and 1-D models were set equal to 0.12 nm. For the tight-binding calculations on the 1-D model **4**, a set of 51 k points was used. In the case of the 2-D nonmetal networks, 36 k points, chosen in the rectangle irreducible part of the Brillouin zone, were used. The plot of the band structure of the regular 2-D light atoms layers was also made using the conventional rectangle unit cell (Z = 2), in order to compare with the nonregular ones. The group of k along the different lines were C_{2v} in the regular net and either C_{2v} or C_s in the distorted ones. For the calculations on the 3-D $Gd_2B_3C_2$ material, a set of 16 k points was chosen in the irreducible wedge of the Brillouin zone, corresponding to the conventional simple orthorhombic cell (Z = 2). All k point sets were chosen in accordance with the geometrical method described by Ramirez and Böhm.[16]

Metallography and Homogeneous Range

The stoichiometric composition of $Gd_2B_3C_2$ (28.6–42.8–28.6 atom %) is quite close to the composition REB_2C, for which two different boride–carbide structure types have been observed so far. The smaller RE metals from Tb through Lu and Sc adopt the YB_2C structural type,[5] whereas CeB_2C crystallizes with the ThB_2C-type.[7]

To detect the possible formation of any of these phases and to check on a possible homogeneity range for $Gd_2B_3C_2$, careful lattice parameter measurements and metallography were carried out on various arc melted and annealed samples near the stoichiometric composition. The results show that there is no formation of a REB_2C compound in the Gd–B–C system. Samples prepared at the nominal compositions of 25-50-25 or 25-45-30 atom %, respectively, show the presence of $Gd_2B_3C_2$ in equilibrium with GdB_4 and GdB_2C_2 in the as-cast state as well as after annealings at 1400 and 1000 °C, confirming this three-phase region earlier observed by Smith and Gilles[9] (see micrograph a in Figure 1). At the stoichiometric composition $Gd_2B_3C_2$ is observed in a single-phase condition, indicating congruent melting without decomposition or phase transformation between 1000 °C and the melting point (see Figure 1b). At the equiatomic composition "GdBC", however, a two-phase lamellar microstructure is observed (see Figure 1c). The X-ray powder patterns show only a few nonindexed lines, belonging very probably to "Gd_2BC_2", as indicated by Smith and Gilles.[9]

Table 4 shows the lattice parameters observed in various samples after annealing at 1400 °C. The arc melted alloys and those annealed at 1000 °C show virtually the same parameters within the experimental error. The only difference observed is a decrease of the cell volume of GdB_4, indicating a significant increase of carbon solubility at higher temperatures.

On the basis of the synthetic composition, with an estimated error of 10% of each atomic fraction Smith and Gilles[9] assigned the formula $Gd_{0.3}B_{0.4}C_{0.3}$ for the present phase $Gd_2B_3C_2$. In view

(13) Rogl, P.; Rupp, B.; Felner, I.; Fischer, P. *J. Solid State Chem.* **1993**, *104*, 377.
(14) (a) Whangbo, M.-H.; Hoffmann, R. *J. Am. Chem. Soc.* **1978**, *100*, 6093. (b) Whangbo, M.-H.; Hoffmann, R.; Woodward, R. B. *Proc. R. Soc. London Ser. A* **1979**, *366*, 23.
(15) Hoffmann, R. *J. Chem. Phys.* **1962**, *39*, 1397.
(16) Ramirez, R.; Böhm, M. C. *Int. J. Quantum Chem.* **1986**, *30*, 391.

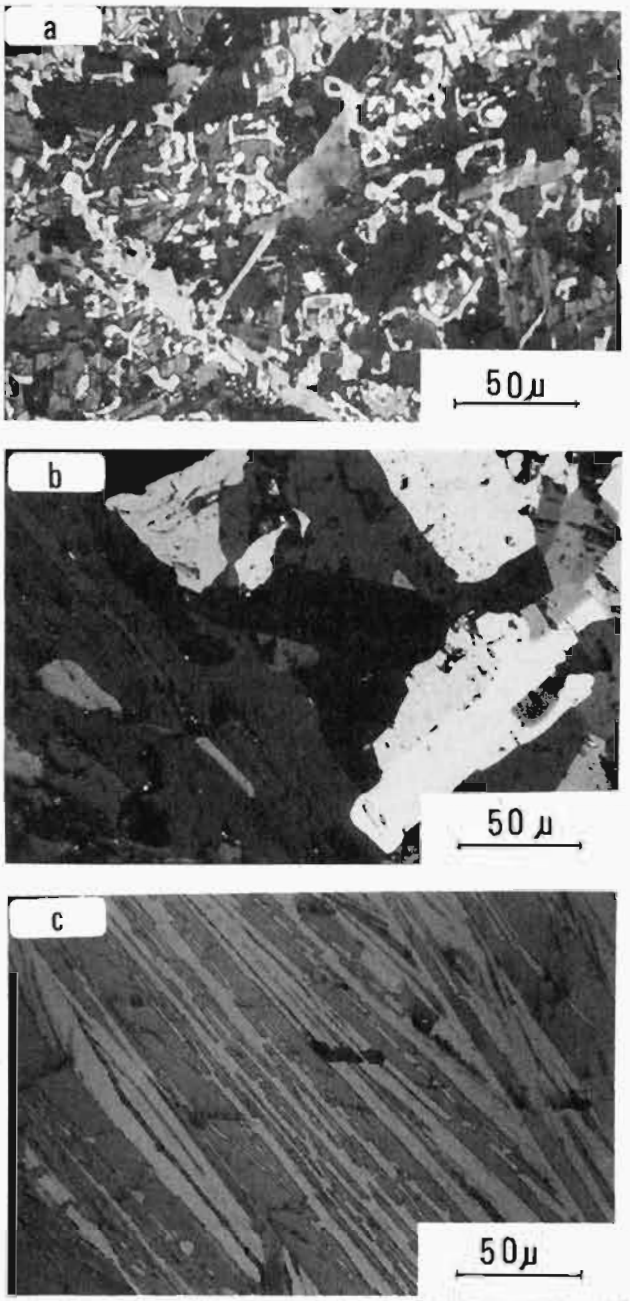

Figure 1. Micrographs near the composition $Gd_2B_3C_2$: (a) "GdB_2C" three-phase region $Gd_2B_3C_2$–GdB_2C_2–GdB_4; (b) single-phase $Gd_2B_3C_2$ region; (c) two-phase region $Gd_2B_3C_2$–Gd_2BC_2 with lamellar crystallization at the equiatomic composition "GdBC".

of the correct formula $Gd_{0.286}B_{0.428}C_{0.286}$ their estimation was very good. However, the range of 10% of each atomic fraction should not been misunderstood as the homogeneity range of $Gd_2B_3C_2$. In this work we have not observed any significant change of the lattice parameters or the cell volume of $Gd_2B_3C_2$ (see Table 4) clearly classifying this boride carbide as a truely stoichiometric compound in consistency with the ordered covalent nature of the boron–carbon layers described below.

Structural Chemistry

The crystal structure of $Gd_2B_3C_2$ is a unique structure type, however, closely related to the crystal structure of YBC.[4] Infinite boron zigzag chains branched with carbon atoms are common to both structure types. Boron atoms B1 in $Gd_2B_3C_2$, as usual for most transition metal borides,[17] are in triangular prismatic metal coordination with typical bond angles in the chain of $\varphi_{B1-B1-B1}$ = 127.6° (see Figure 2). The chains are running parallel to the *a* axis of the unit cell and are branched with carbon atoms. With three nonmetal atoms (2B1 + C) around the waist of the metal prism, the overall coordination around each boron B1 atom increases to nine atoms: $B1^{[6Gd+1C,2]}$. Branched carbon atoms are in 4-fold rectangular and almost quadratic (c/a = 1.077) metal coordination at a distance of d(B1–C) = 0.1597 nm from the boron chain under bond angles of $\varphi_{C-B1-B1}$ = 116.2°. Thus far (see Figure 2) the description of the crystal structure of $Gd_2B_3C_2$ matches the one for YBC.[4] A striking difference with respect to the nonmetal sublattice of YBC is the linkage of the carbon branched boron zigzag chains in $Gd_2B_3C_2$ by additional boron atoms B2 engaged in rather tight and straight bonds (φ_{C-B2-C} = 180°, d(B2–C) = 0.1413 nm) with the two carbon atoms of the two chains linked, thereby forming a planar two-dimensional boron-carbon framework, as the essential new feature of the unique $Gd_2B_3C_2$ type (see Figure 2). A simple comparison of the structural chemical formulas reveals the prominent differences between the two related structure types: $Gd_2B_2^{[6Gd+C,2B]}B^{[2C,-]}C_2^{[4Gd+2B,-]}$ and $YB^{[6Y+C,2B]}C^{[4Y+B,-]}$. [The additional boron atom linking the branched boron–carbon chains does not change much in the X-ray powder intensities, and so 20 years ago $Gd_2B_3C_2$ was mistaken by J.B. for "GdBC".[4]] Comparing the nonmetal bond distances (see Table 3) we see rather tight bonding among the straight B1–C–B2–C–B1 units, whereas B1–B1 intrachain distances of 0.192 nm are certainly at the upper limit of covalent B–B bond distances. The rather strongly bonded units B1–C–B2–C–B1 running parallel to the *b* axis may explain the reduced *b* value with respect to the relatively large *b* values of the Tb, Dy, and Y members of the series crystallizing in the YBC-type[4] where B2 atoms are missing and no such contacts are effective. Whereas boron–carbon chains of various lengths and with various bond angles have been observed in the crystal structures of cerium and lanthanum boron carbides,[1,5] tightly bonded and straight single C–B–C groups with similar bond distances are the characteristic structural element of the Sc_2BC_2-type[18] as a further representative of the diversified structural chemistry of the rare earth metal boride carbides. Analogous triatomic units are also encountered in other solid-state compounds.[19]

Electronic Structure

Ternary metal boride carbides $M_xB_yC_z$ can be classified in three different families according to the dimensionality of the boron–carbon network, which is related to the averaged valence electron count (VEC) per main group atom.[1] In the case of $Gd_2B_3C_2$, assuming a complete electronic transfer from the trivalent gadolinium element to the boron-carbon net, the VEC is $(3 \times 2 + 3 \times 3 + 4 \times 2)/5 = 4.6$. This compound belongs to the class of materials having a VEC less than 5.0 and exhibiting 2-D nonmetal layers alternating with 2-D metal sheets. However, according to the metal-metal separations measured in the title compound (see Table 1), metal–metal bonding seems present and the electron transfer from the metal atoms towards the light atoms could be incomplete. The question which arises then is the following: what is the formal oxidation state of the metal atoms and the boron–carbon net?

Extended Hückel calculations have been performed in order to understand the bonding in the title compound. We first analyze

(17) Rogl, P. Formation and Crystal Chemistry of Metal Borides. In *Inorganic Reactions*, Zuckerman, J. J., Ed.; Verlag Chemie: Weinheim, Germany, 1991; Vol. 7.
(18) Halet, J.-F.; Saillard, J.-Y.; Bauer, J. *J. Less-Common Met.* **1990**, *158*, 239.
(19) (a) Down, M. G.; Haley, M. J.; Hubberstey, P.; Pulham, R. J.; Thunder, A. E. *J. Chem. Soc. Dalton Trans.* **1978**, 1407. (b) Yamane, H.; Kikkawa, S.; Horiuchi, H.; Koizumu, M. *J. Solid State Chem.* **1986**, *65*, 6. (c) Yamane, H.; Kikkawa, S.; Koizumu, M. *J. Solid State Chem.* **1987**, *71*, 1. (d) Evers, J.; Munsterkotter, M.; Oehlinger, G.; Polborn, K.; Sendlinger, B. *J. Less-Common Met.* **1990**, *162*, L17. (e) von Schnering, H. G.; Somer, M.; Hartweg, M.; Peters, K. *Angew. chem., Int. Ed. Engl.* **1990**, *29*, 65.

Table 4. Unit Cell Dimensions (nm) of the Phases Observed in the Neighborhood of $Gd_2B_3C_2$ (Noting that the Lattice Parameters Measured by the Guinier–Huber Method Are Usually Slightly Smaller Than Those Obtained by Single-Crystal Techniques)

	weighed in compositions Gd–B–C atom %							
	25–50–25 ("GdB_2C")			25–45–30			28.6–42.8–28.6 ($Gd_2B_3C_2$)	33.3–33.3–33.3[a] ("GdBC")
phase	$Gd_2B_3C_2$	GdB_2C_2	GdB_4	$Gd_2B_3C_2$	GdB_2C_2	GdB_4	$Gd_2B_3C_2$	$Gd_2B_3C_2$
a, nm	0.34329(5)	0.3787(1)	0.71298(7)	0.34338(4)	0.38007(8)	0.7140(5)	0.34337(5)	0.34336(6)
b, nm	1.36977(9)			1.3701(4)			1.3702(4)	1.3698(3)
c, nm	0.37006(5)	0.7278(3)	0.40461(8)	0.37011(5)	0.7308(2)	0.4021(4)	0.37014(5)	0.37017(5)
V, nm^3	0.17401(4)	0.10439(9)	0.2057(1)	0.17412(5)	0.10556(5)	0.2050(3)	0.17415(5)	0.17411(5)

[a] A few nonindexed lines probably belong to "Gd_2BC_2".

Table 5. Overlap Populations and Atomic Net Charges Computed for Different Electron Counts in $M_2B_3C_2$.

valence electron count per metal atom	1	3[a]	5
electron count per unit cell	38	46	54
Fermi level, eV	−10.88	−8.99	−6.89
Overlap Populations			
(a) Boron–Metal and Carbon–Metal			
Gd–B1 (0.2738 nm)	0.06	0.15	0.16
Gd–B1 (0.2787 nm)	0.06	0.09	0.09
Gd–C (0.2568 nm)	0.15	0.17	0.14
(b) Metal–Metal			
Gd–Gd (0.3615 nm)	0.02	0.09	0.09
Gd–Gd (0.3689 nm)	0.00	0.04	0.23
Gd–Gd (0.3711 nm)	0.02	0.01	−0.01
(c) Boron–Boron and Boron–Carbon			
B2–C (0.1413 nm)	1.20	1.22	1.21
B1–C (0.1596 nm)	0.93	0.81	0.79
B1–B1 (0.1920 nm)	0.52	0.69	0.70
Atomic Net Charges			
Gd	+0.12	+1.24	+1.66
B1	+0.63	+0.10	−0.32
B2	+0.63	+0.38	+0.24
C	−1.07	−1.33	−1.45

[a] Electron count for Gd.

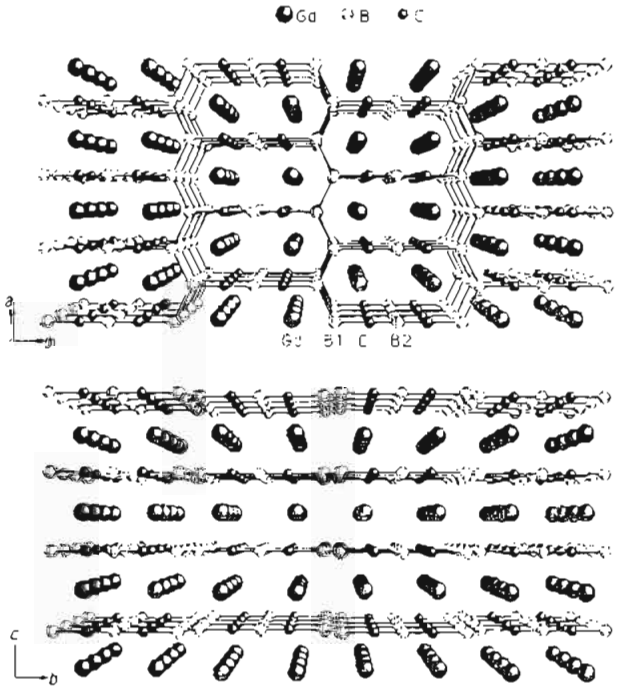

Figure 2. Projection of the crystal structure of $Gd_2B_3C_2$ along the *c* axis (top) and *a* axis (bottom). Large circles are Gd, small open circles are boron atoms, small filled circles are carbon atoms.

the bonding in each of the nonmetal and metal layers. In a second step, the electronic structure of the 3-D material is described.

(a) The Boron–Carbon 2-D Net. The 2-D boron–carbon net shown in Figure 2 can be considered to result from the assembly of linear conjugated units B1–C–B2–C–B1 which are linked together through B1–B1 single bonds, in which the B1 atoms adopt the sp^2-type coordination mode. Therefore, we start the analysis by investigating the electronic structure of the simplest molecular analog of this basic building block, namely $[H_2BCBCBH_2]^{n-}$ (**1**) and by determining the preferred anionic charge *n* favoring the planar D_{2h} structure **1** over the nonplanar D_{2d} arrangement **2**.

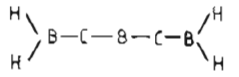

1

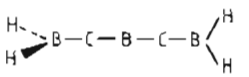

2

The Walsh diagram corresponding to the $D_{2d} \rightarrow D_{2h}$ transformation is shown in Figure 3, together with the corresponding total energy variation of $[H_2BCBCBH_2]^{n-}$ for different values of *n*. In these calculations, all the B–C bond lengths were set at 0.15 nm. With a charge of 3–, the planar structure **1** is less stable than the nonplanar arrangement **2** (by 0.11 eV). Such an arrangement is in fact observed for its isoelectronic organic analog, the pentatetraene $H_2C{=}C{=}C{=}C{=}CH_2$.[20] On the other hand, the planar structure is strongly preferred for a charge of 5– (by 1.15 eV). In that case, the 4e level of **2** would be half-occupied, rendering the system Jahn–Teller unstable. A HOMO–LUMO gap of 1.47 eV is calculated between the b_{2u} (π_3) and b_{3g} (π_4) MO's in **1**. With such a charge, the Lewis formulas proposed in **3** show B1–C and B2–C bonds with formal average bond orders of 1.5 and 2.0, respectively. This is consistent with the bonding or nonbonding character of the three π doublets (b_{2u}, b_{3g}, and b_{2u}, respectively) and the two π_σ doublets (b_{3u} and b_{2g}) (see Figure 3a). Accordingly, though the B1–C and B2–C separations were set equal in our model, the calculated overlap population is 1.07 in the former and 1.24 in the latter for the charge of 5–. This is in agreement with the fact that the measured B1–C distances are longer than the B2–C ones (0.159 vs 0.141 nm). For the charges of 4– and 6–, the planar structure **2** is also preferred, but to a less extent. In addition, in the case of $n = 6$, the calculated B–C overlap populations are not in so good agreement with the observed B–C distances as for $n = 5$, due to the partial occupation of the antibonding b_{3g} MO.

Thus, it appears that a formal charge of 5– per B_3C_2 unit explains quite well the planar structure of the nonmetal nets in $Gd_2B_3C_2$, as well as the B–C bond distances. However, the Lewis formulas in **3** suggest an sp^2 hybridization for at least one C atom, while the B1–C–B2–C–B1 units are perfectly linear in $Gd_2B_3C_2$. The calculations indicate that, for the charge of 5–, the linear form is more stable than any bent structure. This preference for the linearity is due to the difference in the electronegativities of carbon and boron. A similar effect has been observed for the linear $[B_2C]^{4-}$ entity, which is the repeat unit in the nonmetal 2-D network in MB_2C compounds.[1] From this MO analysis of the B_3C_2 building block of the boron–carbon 2-D net, we can conclude that its favored electron count

(20) See, for example: Liang, C.; Allen, L. C. *J. Am. Chem. Soc.* **1991**, *113*, 1873. Note that the carbon skeleton of the pentatetraene molecule is slightly bent.

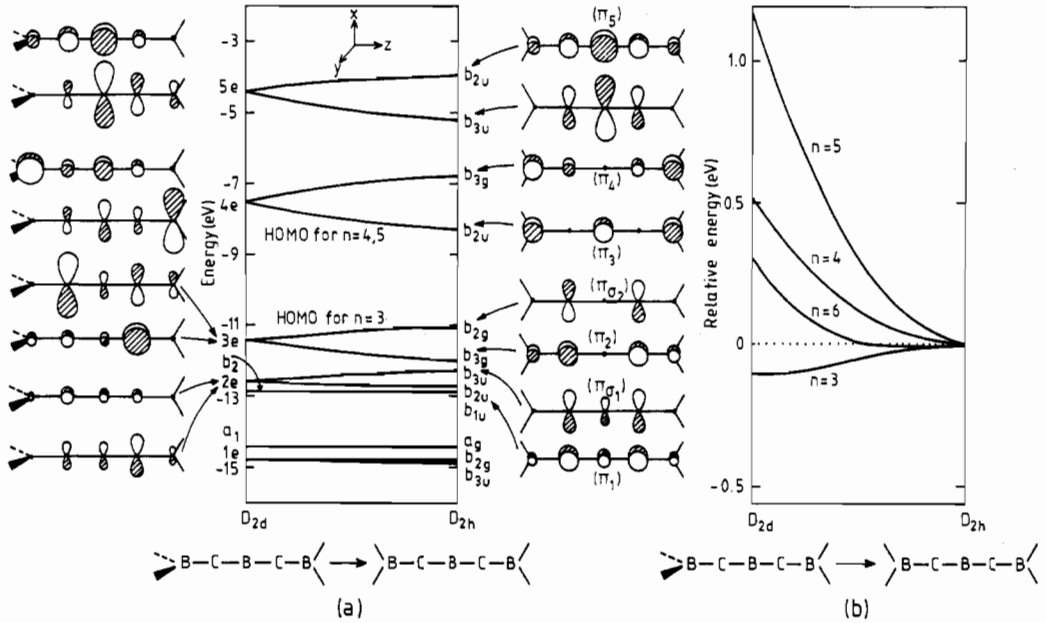

Figure 3. Extended Hückel Walsh diagram (a) and total electronic energy variation (b) for the D_{2d} (nonplanar) → D_{2h} (planar) transformation of the molecular model $[H_2BCBCBH_2]^{n-}$.

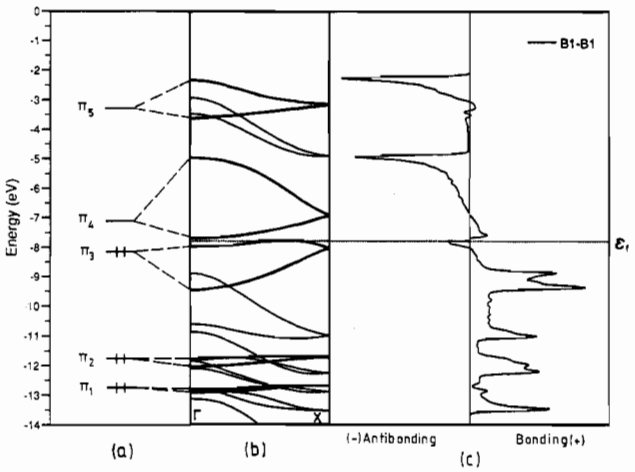

Figure 4. π MO levels of the $[B_3C_2]^{5-}$ repeating unit (a), band structure (b), and B1–B1 COOP curve (c) for the 1-D model **4**.

corresponds to a formal ionic charge of 5– per repeat unit. This formal electron partition leads to the presence of one electron per Gd_2 in the 5d metallic levels (i.e. $Gd^{2.5+}$).

3

In the title compound, the B_3C_2 building blocks are assembled together in such a way as to form infinite sp^2 boron zigzag chains. In order to analyze the bonding in these chains, calculations have been first performed on the 1-D model **4**, based on the $[B_3C_2H_2]^{5-}$ repeating unit, which is electronically related to the molecular model $[B_3C_2H_4]^{5-}$ (**3**). In particular, it presents exactly the same set of π-type levels as **3** (see π_1 to π_5 MO's in Figure 3a). The band structure of **4** is shown in the middle of Figure 4. The existence of a 2_1 screw axis in this 1-D model causes a band degeneracy at $k = \pi/a$, in such a way that each orbital of the $[B_3C_2H_2]^{5-}$ repeat unit generates a folded (double) band. The lower branch of each folded band is (more or less) B1–B1 bonding, while the upper branch is (more or less) B1–B1 antibonding. The bands generated by π_1 and π_2 are flat, due to their small coefficient on B1. This is not the case for the bands derived from π_3 and π_4, which are more dispersed. Since the π_3 and π_4 orbitals of the $[B_3C_2H_2]^{5-}$ repeat unit are both primarily boron-localized and close in energy, they mix significantly in **4**. This mixing can be viewed as a second-order interaction which is stronger in the energy range where the two corresponding bands are close together. As a result, the top of the π_3 band loses most of its B–B antibonding character, while the bottom of the π_4 band loses most of its B–B bonding character. This is illustrated in Figure 4c, which represents the B–B overlap population plotted as a function of the energy (COOP curve).[21] As one can see, the top of the π_3 band is weakly antibonding, while the bottom of the π_4 band is weakly bonding.

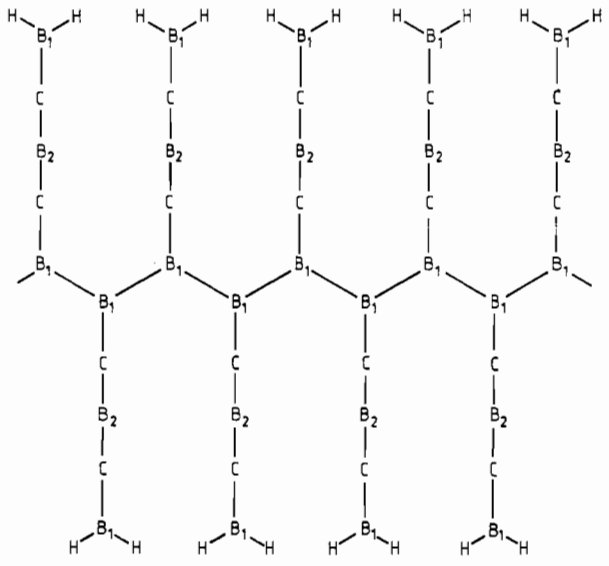

4

When 1-D $[B_3C_2]^{5-}$ boron chains, such as **4**, are assembled to generate the 2-D nonmetal net of $Gd_2B_3C_2$, additional B1···B1 through-bond interactions lead to a broadening of the π_3 and π_4 bands. As a consequence, the small HOMO/LUMO gap present

(21) (a) Hughbanks, T.; Hoffmann, R. *J. Am. Chem. Soc.* **1983**, *105*, 3528.
(b) Wijeyesekara, S. D.; Hoffmann, R. *Organometallics* **1984**, *3*, 949.
(c) Kertesz, M.; Hoffmann, R. *J. Am. Chem. Soc.* **1984**, *106*, 3483.

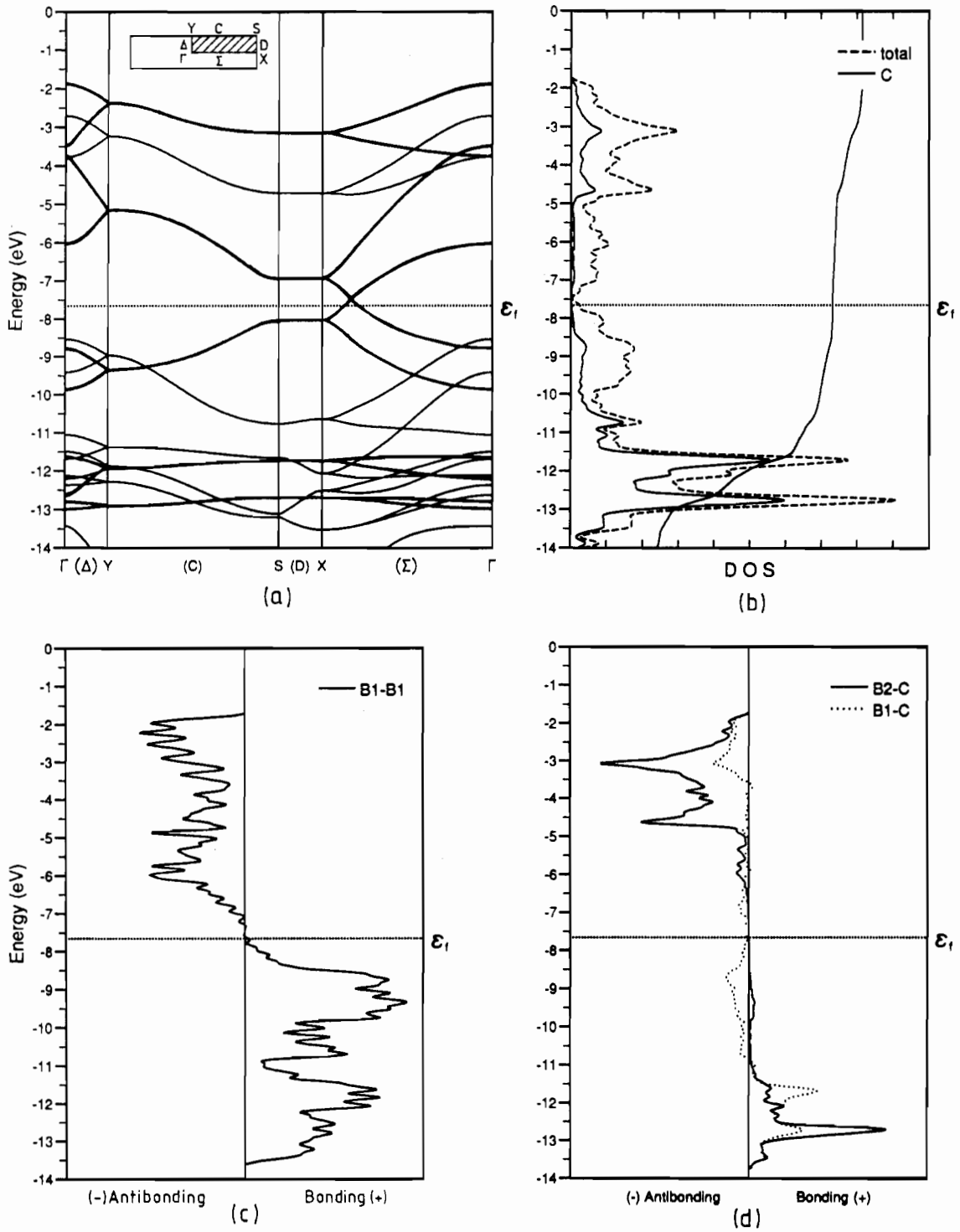

Figure 5. Band structure (a), total and carbon-projected DOS (b), B1–B1 COOP curve (c), and B–C COOP curves (d) in the 2-D nonmetal net of $Gd_2B_3C_2$. The Fermi level corresponds to a charge of 5– per B_3C_2 unit.

in **4** vanishes in the 2-D net. It follows that the corresponding band structure and density of states (DOS) curves (see Figure 5a,b) exhibit a semimetallic feature, with the Fermi level (–7.66 eV) lying in a very deep, almost zero, minimum in the DOS. Moreover, the increase in the dimensionality when going from **4** to the 2-D $[B_3C_2]^{5-}$ net induces an additional mixing between the π_3 and π_4 bands. This mixing transforms the weakly antibonding character of the upper part of the π_3 band into a weakly bonding one. Similarly, the lower part of the π_3 band becomes weakly antibonding. This causes the B1–B1 overlap population to change its sign, not twice as in **4** (see Figure 4c), but only once, very close to the Fermi level where the two bands are touching each other, as shown by the B1–B1 COOP curve (see Figure 5c). As one can see in Figure 5d, the B1–C COOP curve is already largely antibonding below the Fermi level. This is a typical situation in the nonmetal sublattices of metal boride carbides.[1] It indicates that the topology of the net is driven by B–B rather than B–C interactions. For the considered electron count, the computed B1–B1, B2–C, and B1–C averaged overlap populations are 0.94, 1.35, and 0.84, respectively. The ordering of the B–C values reflects the observed bond distances. The analysis of the charge distribution leads to a count of 6.00 π-type electrons per $[B_3C_2]^{5-}$ unit in complete agreement with the Lewis formula proposed in **3**.

At this point of the discussion, the possibility of B1–B1 bond alternation in the $[B_3C_2]^{5-}$ 2-D net has to be considered. Indeed,

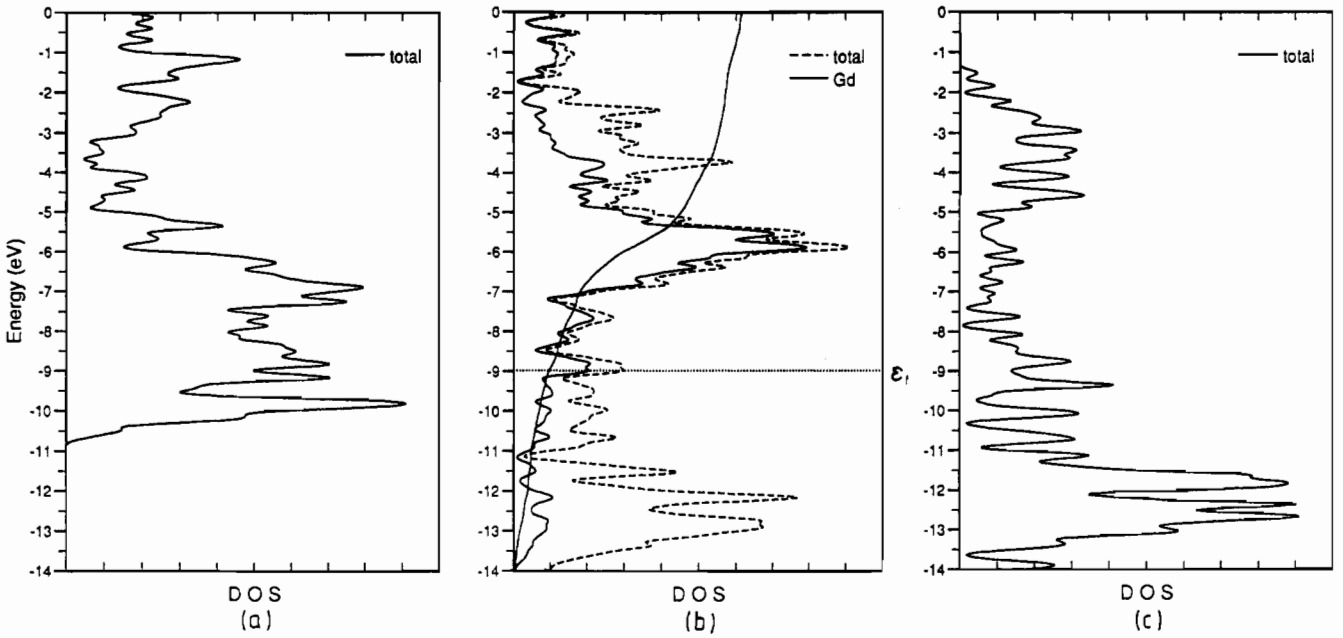

Figure 6. (a) Total DOS for the metallic sublattice before interaction. (b) Total DOS (dashed line) and metallic contribution (solid line) for the material $Gd_2B_3C_2$. (c) Total DOS for the boron–carbon sublattice before interaction.

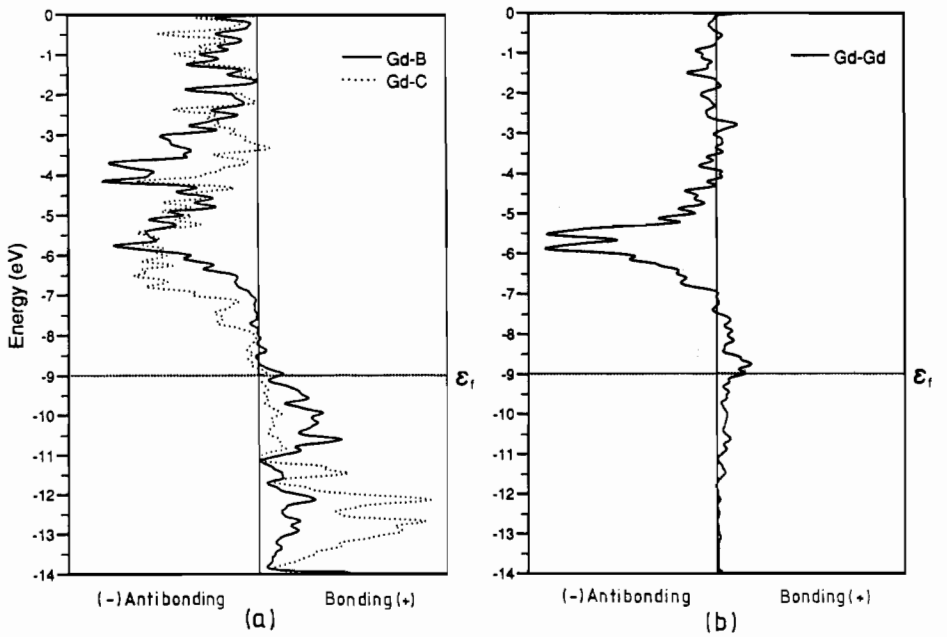

Figure 7. COOP curves for the Gd–B and Gd–C (a) and Gd–Gd (b) contacts in $Gd_2B_3C_2$. The overlap populations have been averaged on all the nonsymmetry-equivalent bonds of the same type.

the Lewis structures **5** and **6** could also account for the 2-D arrangement of $[B_3C_2]^{5-}$, and one could argue that the X-ray structure determination might have missed such a bond alternation feature. A distortion of the regular boron chains is expected to open a gap at the Fermi level. However, as said previously, the involved levels have a poor localization on the B1–B1 bonds and are hardly perturbed by a change in the B–B bonding. As a result, the distorted structures do not appear specially favored, as shown by calculations on **5** and **6**: for a B–B bond length difference of 0.02 nm, the energy change is not significant (less than 0.03 eV per B_3C_2 unit). In the case of **5** a very small gap of 0.3 eV is opened at the Fermi level, while no gap at all is created for **6**. Therefore, if a slight bond alternation in the boron chains cannot be fully ruled out from the flatness of the associated potential energy surface calculated for the 2-D model, it is likely that the preference for regular chains would be reinforced in the real 3-D $Gd_2B_3C_2$ structure.

Although all our results converge to suggest that the formal oxidation state of the nonmetal 2-D net corresponds to a charge of 5– per B_3C_2 unit, we have investigated the possibility of a fully oxidized metal, i.e. a $[B_3C_2]^{6-}$ unit. For such an electron count, assuming a regular net corresponding to the Lewis structure **7**, the Fermi level (–5.96 eV) lies in a range where the states are antibonding on all the bonds. The computed B1–B1, B2–C, and B1–C averaged overlap populations are 0.88, 1.32, and 0.79, respectively. These values are not in as good of an agreement with the experimental bond distances as those calculated for the charge of 5–. Other Lewis structures, namely **8** and **9**, in which one over four B–B bonds is shorter, can also account for this electron count. As for the other electron count, our model calculations indicate that the distorted structures are not likely to be more stable than the regular one.

(b) The Material $Gd_2B_3C_2$. The total DOS (dashed line) and its metallic contribution (solid line) computed for the compound $Gd_2B_3C_2$ are illustrated in the middle of Figure 6. The DOS of $Gd_2B_3C_2$ is not simply the superposition of the DOS of the metallic

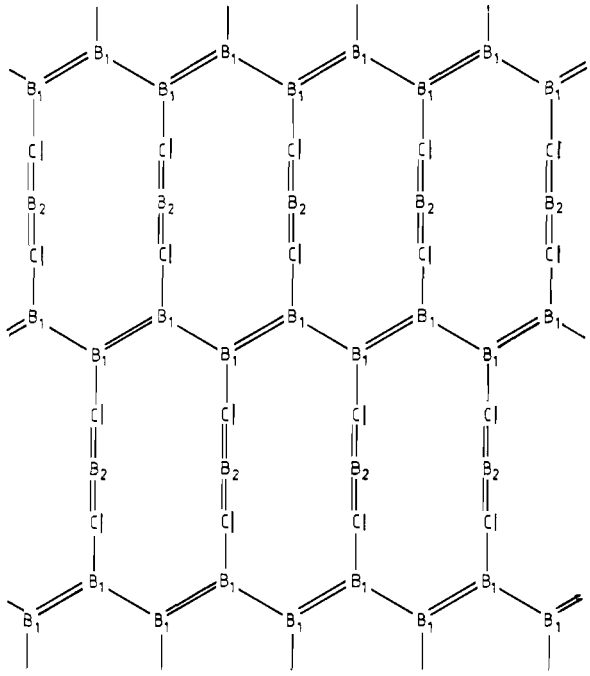

5

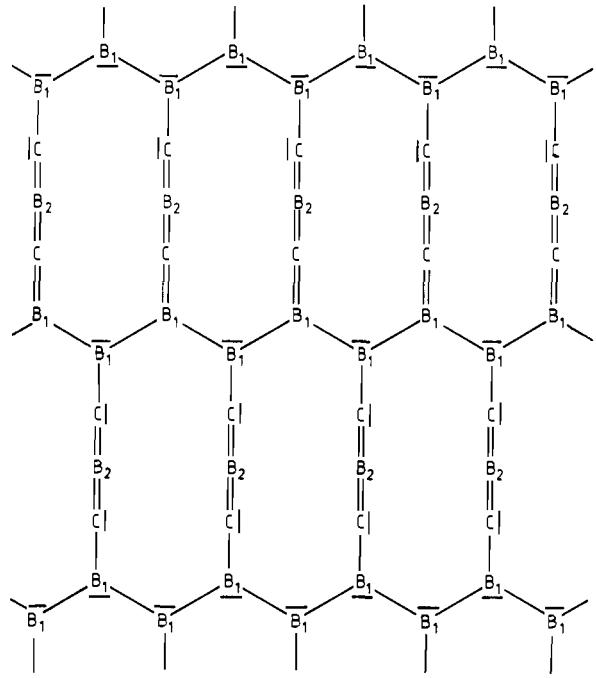

7

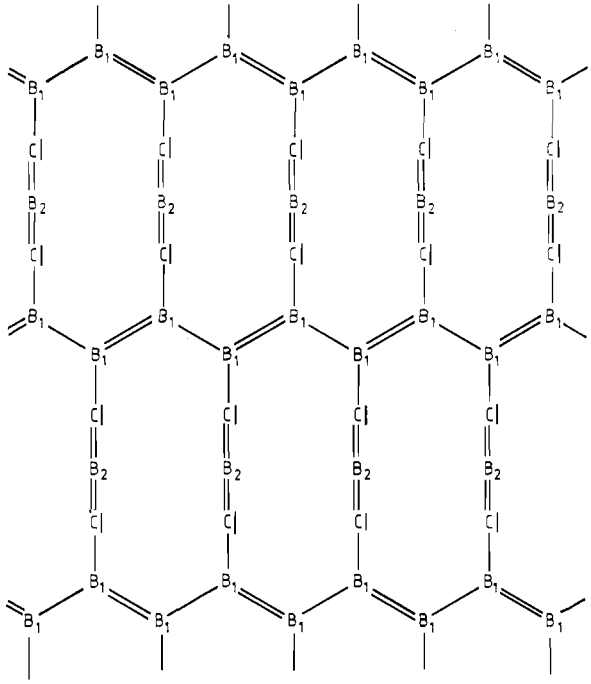

6

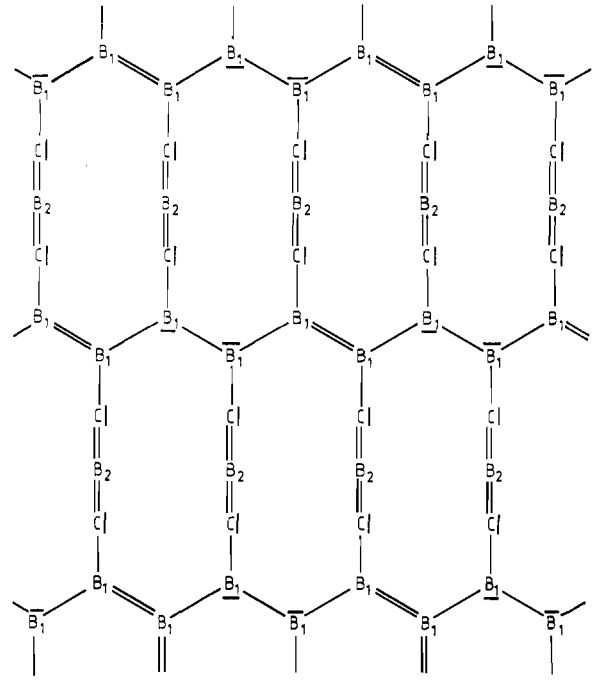

8

framework and the boron–carbon framework before interaction, shown on the left and on the right side, respectively. The shape of the metallic DOS is very different before and after interaction with the boron–carbon layers. Some covalent interaction occurs between the two networks. This is seen in the rather important metallic contribution present in the lower part of the DOS, which derives mainly from the nonmetal network. Consequently some electron transfer occurs from the anionic boron–carbon nets toward the cationic metal atoms. The computed atomic net charges are the following:

$$[Gd^{1.24+}]_2[(B1)^{0.10-}]_2[(B2)^{0.38+}](C^{1.33-})_2$$

It is noteworthy that the boron atoms forming the zigzag chains (B1) are slightly charged negatively, while the ones linking the chains (B2) are slightly positive. This was already observed before interaction with the metallic sublattice. This is interesting for evaluating possible substituent effects. For example, if some C atoms replace some B atoms, they will enter the sites with greater electron density, i.e. the B1 positions.

The rather important peak of DOS cut by the Fermi level at −8.99 eV, consists of both metal and boron–carbon states. This indicates clearly that $Gd_2B_3C_2$ should be isotropically metallic. The overlap populations between metal and light atoms are also a good indicator of the covalent character encountered in this material. The COOP curves associated with all the Gd–B and Gd–C contacts are shown in Figure 7. These averaged overlap populations reach or are very close to their maximum values, which are highly positive. Assuming a rigid band model, we see in Table 5 that removing electrons (i.e. changing the valency of the metal element in $M_2B_3C_2$) leads to a weakening of the M–B and M–C bonds. On the other hand, the adding of extra metallic

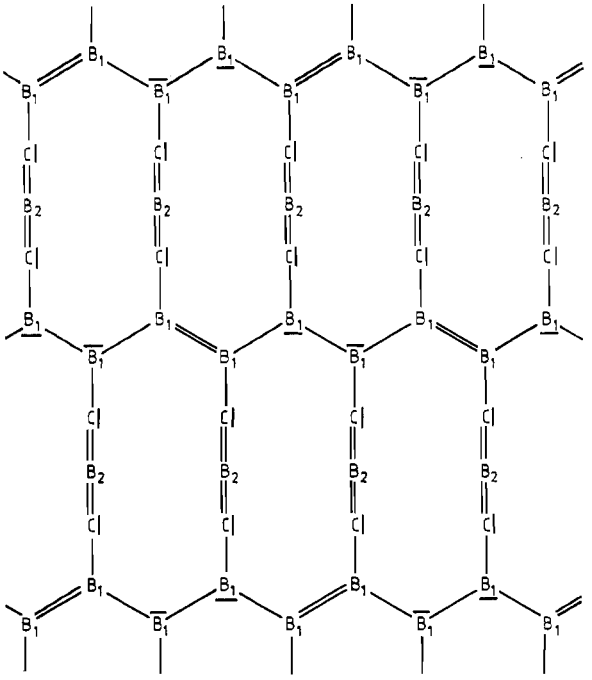

9

electrons almost do not perturb them. It also hardly affects the B–B and B–C bonds (see Table 5). As expected, a weakening of the B–B and B–C overlap populations is noticed after interaction. This is the result of electron donation to the metal atoms.

The COOP curves corresponding to the Gd–Gd contacts (see Figure 7) show that the metal–metal interaction is overall bonding. Positive values are computed for the corresponding overlap populations (see Table 5). The relative importance of the overlap populations is mainly due to the fact that the sites which are populated near the Fermi level present a high metallic contribution (see Figure 6). Our calculations suggest that a stronger metal-metal bonding would emerge with more electrons in the d band (see Table 5 and Figure 7). It would be interesting to see if the $M_2B_3C_2$ structure is possible with metallic elements richer in electrons than Gd like Ce or Th. One should note, however, that phase diagram studies in Ce–B–C[7] and An–B–C (An = Th, U, Pu)[3] systems revealed no indication for the formation of isotypic $M_2B_3C_2$-type compounds.

Acknowledgment. Thanks are expressed to D. Minier for help in the sample preparation, to Y. Piel for the superb preparation of the micrographs, to H. Guérin for the photographs, to G. Elin for typing delicate parts of the manuscript, and to L. Hubert for the drawings. P.R. is grateful to the Austrian Academy of Sciences for a research grant at the INSA, Rennes, France. F.W. thanks the Région Bretagne for financial support.

Supplementary Material Available: Tables giving atom coordinates and anisotropic thermal parameters and powder intensity data for $Gd_2B_3C_2$ (2 pages). Ordering information is given on any current masthead page.